Shaping finite-energy diffraction- and attenuation-resistant beams through Bessel-Gauss–beam superposition

M. Zamboni-Rached* and Mo Mojahedi

Department of Electrical and Computer Engineering at the University of Toronto, 10 King's College street, Toronto, Ontario, Canada

(Received 28 June 2015; published 29 October 2015)

In this paper we develop an analytical method for spatial shaping of diffraction- and attenuation-resistant beams carrying finite power in absorbing media. This can be achieved through suitable discrete superposition of Bessel-Gauss beams, where the approach can be seen as an extension of the frozen wave method, without the inconvenience of infinite power flux and spatial periodicity of the resulting beams.

DOI: 10.1103/PhysRevA.92.043839 PACS number(s): 42.60.Jf, 42.25.Fx, 42.25.Bs

I. INTRODUCTION

Previously a method for spatial modeling of diffraction- and attenuation-resistant beams in absorbing media was developed in Ref. [1]. In general terms, the method allows for obtaining a beam of light, resistant to attenuation and diffraction, with a longitudinal intensity pattern that can be chosen *a priori* [1–4]. This method, named frozen wave (FW), consists of suitable superposition of copropagating equal order Bessel beams, where its experimental confirmation for nonabsorbing media can be found in [5,6].

Despite the fact that the FW method provides impressive results, the derived exact analytical solutions possess infinite power flux and, in the case of nonabsorbing media, they also present an undesired spatial periodicity along the beam direction of propagation. It goes without saying that the aforementioned unphysical behaviors do not appear in the actual experiments due to the finite size of the aperture needed to generate the beams. However, for both theoretical and better understanding of the experimental results, it is necessary to develop an analytical description of the FWs with finite power flux and without spatial periodicity along the direction of propagation. These goals can be achieved, for instance, if one changes the kind of Bessel beam superposition used from a discrete to a continuous one. The difficulty in this case lies in performing the necessary integrations which rarely furnishes analytical solutions [7]. Another possibility is to perform a spatial truncation on the initial FW field [2], but, in this case, the mathematical difficulties for obtaining analytical solutions are even greater.

In this paper, we present a class of solutions to the aforementioned problems by obtaining a finite power version of the FW beams, in both absorbing and nonabsorbing media, through suitable superposition of discrete Bessel-Gauss beams. Such constructed FWs are resistant to diffraction and absorption and will not display the undesired longitudinal periodicity.

The next section is devoted to a modified version of the usual FW method, by ensuring that the transverse wave numbers of the involved Bessel beams are always real when the material medium is absorbent, something that does not occur in the traditional method [1], where the Bessel beams in loss media possess complex transverse and longitudinal wave numbers. This modified version presents the very same problem of infinite power flux, but it can be more appropriate in dealing with situations where a given FW beam propagating in an absorbing medium is being generated outside it, in a nonabsorbing medium (in air, for instance).

Because it is new, the content of Sec. II is part of the contribution of the present work, whose main contributions are given by Sec. III and (especially) by Sec. IV, where the finite-energy version of the FW method is presented.

II. MODIFIED VERSION OF THE FROZEN WAVE METHOD AND THE MAIN GOALS OF THE PRESENT WORK

A good description of the FWs can be found in Refs. [1–4]; however, here we present a modified version of this approach by requiring that the Bessel beams forming the FW to have real transverse wave numbers. Theoretically, a Bessel beam with complex transverse wave number is possible if the beam is constructed inside a homogeneous absorbing medium through the superposition of plane waves with the wave vectors localized on a cone surface. A Bessel beam with a real transverse wave number in an absorbing medium occurs when, for instance, the beam is generated in a nonabsorbing medium and is partly transmitted to the absorbing medium at normal incidence, something that can occur in many important applications.

Let us consider a linear, isotropic, and homogeneous absorbing medium with complex refractive index given by $n_{\text{ref}} = n_r + i\, n_i$. The basic idea is to shape, within a certain spatial range, the longitudinal intensity pattern of diffraction- and attenuation-resistant beams. We wish the chosen longitudinal intensity pattern to occur over a cylindrical surface of radius $\rho_0 \geqslant 0$. Mathematically, we wish $|\Psi(\rho = \rho_0, \phi, z, t)|^2 \approx |F(z)|^2$, within $0 \leqslant z \leqslant L$. When $\rho_0 = 0$, we also can choose the spot radius (r_0) of the resulting beam. Here, the function Ψ represent, for instance, the transverse Cartesian component of a electrical field of the type $\mathbf{E} = \Psi \hat{x} + E_z \hat{z}$, where E_z can be calculated (in the case of source free, linear, isotropic, and homogeneous media) through the Gauss law, $E_z = -\int \partial_x \Psi \, dz$.

*On leave from DECOM-FEEC, University of Campinas, Campinas, São Paulo, Brazil. Corresponding author: mzamboni@decom.fee.unicamp.br

To achieve the above, the following superposition of equal frequency copropagating Bessel beams of order ν is proposed:

$$\Psi(\rho,\phi,z,t) = \mathcal{N}_\nu\, e^{-i\omega t} \sum_{n=-N}^{N} A_n J_\nu(\eta_n \rho) e^{i\nu\phi} e^{i\zeta_n z}. \quad (1)$$

Here, A_n are constants coefficients and ζ_n and η_n are the longitudinal and the transverse wave numbers (respectively) of the nth Bessel beam in the superposition, related to each other according to

$$\eta_n = \sqrt{k^2 - \zeta_n^2}. \quad (2)$$

In the above expression k is the complex (total) wave number given by

$$k = (n_r + i n_i)\frac{\omega}{c} = k_r + i k_i. \quad (3)$$

In addition, $\mathcal{N}_\nu = 1/[J_\nu(\cdot)]_{\max}$, where $[J_\nu(\cdot)]_{\max}$ is the maximum value of the Bessel function of the first kind $J_\nu(\cdot)$.

It is important to pay close attention to the notation used here: "n" is the summation index in Eq. (1), assuming integer values in the range $-N \leqslant n \leqslant N$, whereas the complex index of refraction is written as $n_{\text{ref}} = n_r + i n_i$, where n_r and n_i are the real and imaginary parts of the index, respectively.

In order to proceed, the following choices for the transverse wave numbers (η_n) and coefficients A_n are made:

$$\eta_n = \sqrt{\left(n_r^2 - n_i^2\right)\frac{\omega^2}{c^2} - \left(Q + \frac{2\pi n}{L}\right)^2 + \left(\frac{\omega^2}{c^2}\frac{n_r n_i}{Q + \frac{2\pi n}{L}}\right)^2}, \quad (4)$$

which implies $\zeta_n = \zeta_{r\,n} + i\,\zeta_{i\,n}$, with

$$\zeta_{r\,n} = Q + \frac{2\pi n}{L},$$
$$\zeta_{i\,n} = \frac{\omega^2}{c^2}\frac{n_r n_i}{\zeta_{r\,n}}. \quad (5)$$

and

$$A_n = \frac{1}{L}\int_0^L F(z) e^{-\left(i\frac{2\pi}{L}n - \zeta_{i\,0}\right)z} dz, \quad (6)$$

where, according to (5), $\zeta_{i\,0} = (\omega^2/c^2) n_r n_i / Q$. Here, Q is a positive constant related to the transverse dimensions of the beam as will be discussed later.

To ensure purely real transverse wave numbers (η_n) and positive values for the real part of the longitudinal wave number,[1] we must have

$$0 \leqslant \zeta_{r\,n} \leqslant \frac{\omega}{c}\sqrt{\frac{\left(n_r^2 - n_i^2\right) + \sqrt{\left(n_r^2 - n_i^2\right)^2 + 4\left(n_r^2 n_i^2\right)}}{2}}. \quad (7)$$

Once Q and L are chosen, expression (7), along with the first equation of (5), provide us with the maximum value of N to be used in (1). The desired longitudinal intensity pattern, $|F(z)|^2$, can now be constructed on axis ($\rho = 0$) or on the surface of cylinder of radius $\rho = \rho_0$ as follows.

(i) In the case of on axis pattern ($\rho = 0$), zero-order Bessel beams (i.e., $\nu = 0$) are used in the fundamental superposition (1). Moreover, through a suitable choice of Q, it is possible to choose the resulting beam's spot radius according to

$$r_0 \approx \frac{2.4}{\eta_0}. \quad (8)$$

(ii) In the case of patterns on the surface of a cylinder of radius $\rho = \rho_0$, higher-order Bessel beams (i.e., $\nu \geqslant 1$) are used in (1). The radius ρ_0 of the cylinder can be approximately chosen if Q is evaluated from

$$\left[\frac{d}{d\rho} J_\nu(\eta_0 \rho)\right]\Big|_{\rho=\rho_0} = 0. \quad (9)$$

The method described above provides a powerful way for modeling diffraction- and attenuation-resistant beams which are useful in many fields such as optical tweezers, optical atom guiding, remote sensing, free space optics communications, and so on. However, the beam solution given by Eqs. (1)–(6) has the drawback of having an infinite power flux. This is particularly evident in the simple case of nonabsorbing media, where the resulting FW beam possesses infinite periodicity (with period L) along the spatial coordinate z. To see this let us consider the following example.

Example 1. Here we will construct two FW beams with the same spot sizes and longitudinal intensity patterns, one of them in a nonabsorbing medium with $n_{\text{ref}} = n_r = 2$ and the other in an absorbing medium with $n_{\text{ref}} = n_r + i n_i = 2 + i\,7.5 \times 10^{-7}$. Both beams have the same optical (free-space) wavelength of $\lambda = c/f = 632.8$ nm, with spot size of radius[2] $r_0 \approx 9\ \mu$m, and with a ladder-shaped longitudinal intensity pattern on the axis. More specifically, we wish that in each medium, within the range of $0 \leqslant z \leqslant L$, the corresponding square beam amplitude to be given by $|\Psi(\rho = 0,z,t)|^2 \approx |F(z)|^2$, with

$$F(z) = \begin{cases} 0 & \text{for } 0 < z < l_1, \\ 1 & \text{for } l_1 < z < l_2, \\ \sqrt{2} & \text{for } l_2 < z < l_3, \\ \sqrt{3} & \text{for } l_3 < z < l_4, \\ 0 & \text{for } l_4 < z < L, \end{cases} \quad (10)$$

where $l_1 = 0.05$ m, $l_2 = l_1 + \delta z$, $l_3 = l_2 + \delta z$, and $l_4 = l_3 + \delta z$, with $L = 0.37$ m and $\delta z = 0.08$ m.

Using the FW method formulated above, Eqs. (1)–(8), with $\nu = 0$, the desired beam patterns are calculated and plotted in Fig. 1. The coefficients A_n (for both cases) are easily calculated in closed analytical form, but are not shown here explicitly. From the desired spot size, the calculated values of Q (for both beams) are approximately the same, $Q \approx 0.99991 k_r = 1.9857 \times 10^7\ \text{m}^{-1}$. Moreover, for both cases, the maximum allowed value of N is 210; however, a good result is already obtained with $N = 40$.

[1] To guarantee only forward propagating Bessel beams in the superposition (1).

[2] Note that a Gaussian beam (in any of the two media) with the same initial spot size doubles its beam size due to diffraction after only 2.8 mm, and that a plane wave, in the absorbing medium, would have a penetration depth of only 6.7 cm.

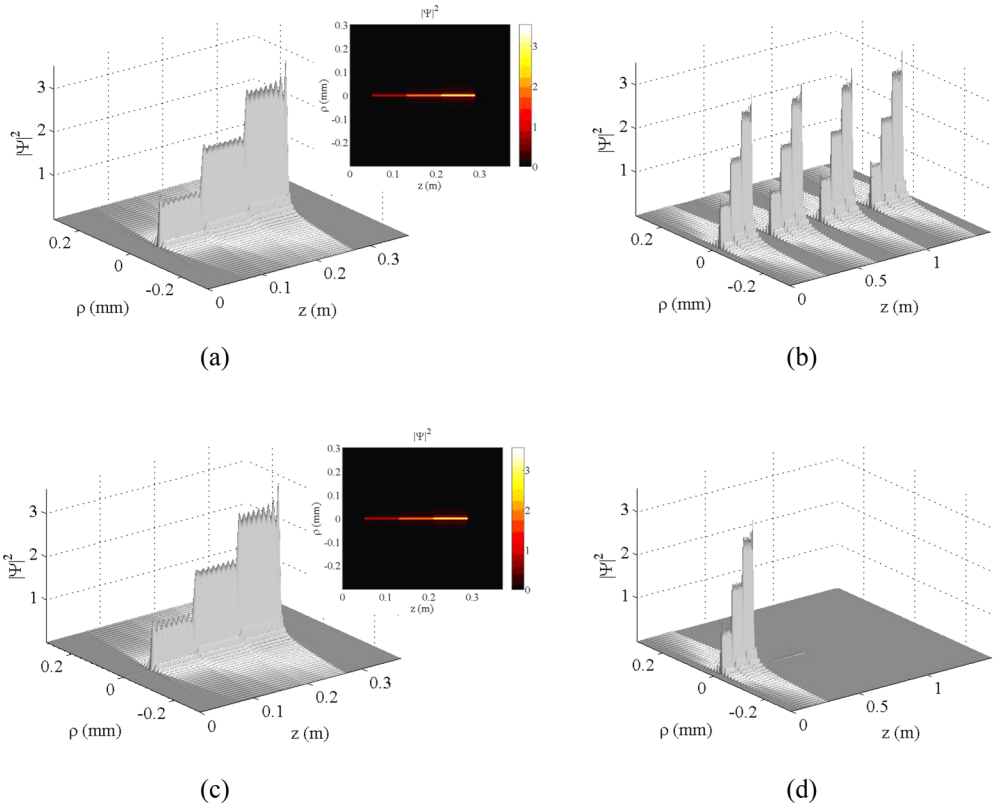

FIG. 1. (Color online) (a) Desired FW beam intensity in the nonabsorbing medium and its orthogonal projection. (b) The same beam as in (a) but over an extended longitudinal range, $0 \leqslant z \leqslant 4L = 1.48$ m, where longitudinal periodicity is evident. (c) The desired FW beam in the absorbing medium and its orthogonal projection. (d) The same beam as in (c) but over a longer longitudinal range, $0 \leqslant z \leqslant 4L = 1.48$ m. Despite absence of the spatial periodicity, the resulting beam carries infinite power.

Figure 1(a) shows the beam pattern in the nonabsorbing medium, where $F(z)$ is given by (10) within the range of $0 \leqslant z \leqslant L = 0.37$ m. The orthogonal projection of the beam in the $\rho - z$ plane is also shown as an inset. Figure 1(b) is a plot of the same beam, but for a longer longitudinal range of $0 \leqslant z \leqslant 4L = 1.48$ m, where the spatial periodicity of the beam pattern is obvious. Figure 1(c) shows the desired FW beam intensity, Eq. (10), and its orthogonal projection within the range $0 \leqslant z \leqslant L = 0.37$ m in the absorbing medium, whereas Fig. 1(d) is the same beam as in Fig. 1(c), but for a longer longitudinal range of $0 \leqslant z \leqslant 4L = 1.48$ m. In this figure, while because of the exponential attenuation caused by the losses the spatial periodicity is not evident; nevertheless, the beam carries infinite power.

In principle, there are two ways to avoid the infinite power problem associated with the FW discussed above. One approach is to use theoretically the same procedure which is used experimentally, i.e., to make a suitable spatial truncation of the transverse FW field on the initial $z = 0$ plane. In such an approach the radius of the finite circular aperture, responsible for the truncation, can be chosen in order to guarantee the desired optical field within the range $0 \leqslant z \leqslant L$ and, at same time, to avoid any spatial periodicity of the beam intensity outside of it. Consequently, to theoretically obtain the solution for the "truncated" FW beams, we need to deal with diffraction integrals. The second approach is to change the summation of the Bessel function in (1) from discrete to continuous. Both of these approaches suffer from the same shortcoming: in most cases, we are faced with complicated integrals making it impossible to obtain a closed analytical solution, forcing us to rely on time-consuming indirect numerical simulations.

In our attempt to acquire a finite energy FW, in Sec. III we apply an interesting result from the paraxial wave theory to obtain an apodized version of the FW solution. Lastly, in Sec. IV, we further modify the apodized beam to achieve the ultimate goal of the finite-energy solution, namely, to provide finite-energy diffraction-resistant beams whose longitudinal intensity pattern can be modeled within a given spatial range, with the added feature of possessing negligible intensity values outside it when compared with the beam's intensity levels in the main range.

III. FROZEN WAVES BEAMS APODIZED BY A GAUSSIAN APERTURE

As stated earlier, in this section we use an interesting result from paraxial optics to obtain a Gaussian apodized version of the FW beams. Consider a paraxial beam propagating in a linear, isotropic, homogeneous, but absorbing medium. The corresponding complex wave function for the monochromatic field is given by

$$\Psi = \exp(ikz)\exp(-i\omega t)E(x,y,z), \tag{11}$$

where the complex envelope E must satisfy

$$\nabla_T^2 E + 2ik\frac{\partial E}{\partial z} = 0. \tag{12}$$

Here, ∇_T^2 is the transverse Laplacian and k is the complex wave number given by (3). It is possible to show that if $E(x,y,z)$ is a solution of (12), then the following function:

$$E_G(x,y,z) = \frac{1}{\mu}\exp\left(-q^2\frac{\rho^2}{\mu}\right)E\left(\frac{x}{\mu},\frac{y}{\mu},\frac{z}{\mu}\right), \tag{13}$$

with $\rho^2 = x^2 + y^2$, $\mathrm{Re}(q) > 0$ (a constant), and

$$\mu = 1 + i2\frac{q^2}{k}z, \tag{14}$$

is also a solution of (12) [8–10].

The important insight from the above result is that every paraxial beam solution possesses its own Gaussian apodized version. From (13) it is easy to see that on the initial $z = 0$ plane, $E_G(x,y,z=0) = \exp(-q^2\rho^2)E(x,y,z=0)$. So, the parameter q regulates the transverse intensity width of the Gaussian apodization ($\Delta\rho_G = 1/\sqrt{2}q$) of the beam on the $z = 0$ plane.

Now, let's apply the above results to the FW solution. To do so, some care must be observed: Eq. (1), with the constraint given by Eq. (2), is an exact solution of the wave equation, whereas the result discussed in this section is valid to solutions subject to the paraxial approximation. However, it can be shown that within the paraxial approximation the FW solution can be written exactly as (1), if the following changes are made:

$$\eta_n = \sqrt{2}k\sqrt{1 - \frac{\zeta_n}{k}}, \tag{15}$$

where the transverse wave number also satisfies

$$\eta_n = \sqrt{2}\sqrt{1 - \frac{1}{k_r}\left(Q + \frac{2\pi n}{L}\right)}\,|k|. \tag{16}$$

Consequently, due to (15), the longitudinal wave number

$$\zeta_n = \zeta_{r\,n} + i\,\zeta_{i\,n} \tag{17}$$

has its real and imaginary parts given by

$$\begin{aligned}\zeta_{r\,n} &= Q + \frac{2\pi n}{L},\\ \zeta_{i\,n} &= k_i\left(2 - \frac{\zeta_{r\,n}}{k_r}\right).\end{aligned} \tag{18}$$

Interestingly, the expressions for all other parameters, including coefficients A_n, remain unchanged. Moreover, if we require that only forward traveling beams are acceptable and the transverse wave number, η_n, is purely real then

$$0 \leqslant Q + \frac{2\pi}{L}N \leqslant n_r\frac{\omega}{c} = k_r. \tag{19}$$

The expression above provides us with the maximum value of N, once Q and L are chosen.

With the paraxial FW beam solution in hand Eqs. (1), (16), (18), and (6), we can obtain the Gaussian apodized version of the FW by writing (1) in the form of (11) and applying (13). Consequently, the finite-energy FW solution can be written as

$$\Psi(\rho,\phi,z,t) = e^{-i\omega t}e^{ikz}\frac{\exp\left(-q^2\frac{\rho^2}{\mu}\right)}{\mu}\exp\left(-ik\frac{z}{\mu}\right) \times \sum_{n=-N}^{N} A_n J_\nu\left(\eta_n\frac{\rho}{\mu}\right)e^{i\nu\phi}\,e^{i\zeta_n\frac{z}{\mu}}, \tag{20}$$

with μ given by Eq. (14). Equation (20) is indeed a superposition of Bessel-Gauss beams.

As stated earlier, the new parameter q regulates the transverse intensity width of the Gaussian apodization at $z = 0$ and its value has to be chosen in order to guarantee that all Bessel-Gauss beams in superposition (20) are diffraction resistant in the desired longitudinal spatial range. But, independent of the choice for q, unfortunately, the present apodized FW cannot yet properly represent the FW beams with the desired properties. This becomes clear with the following example, where for simplicity we have considered a lossless medium.

Example 2. We wish to use (20), along with Eqs. (6), (8), (16), (17), and (18), and assigned values of q, to obtain a diffraction resistant beam with intensity spot radius $r_0 \approx 9\ \mu$m and $\lambda = c/f = 632.8$ nm in a medium with $n_{\mathrm{ref}} = n_r = 2$, where the on-axis longitudinal intensity pattern is approximately equal to $|F(z)|^2$, with $F(z)$ given by (10). We choose a set of increasing values for q, or equally a set of decreasing values for the Gaussian apodization width (10^4, 800, 500, and 200 times the FW spot size). Results are shown in Figs. 2(a)–2(d). From Fig. 2(a) it is clear that the desired ladder-shaped intensity pattern within $0 < z < L = 0.37$ m is obtained very satisfactorily, but, unfortunately, the field intensity at $z > L$ is also high. In the subsequent figures [2(b)–2(d)], as the Gaussian apodization width decreases from 10^4 to 800, 500, and finally 200 times the FW spot size, the field for $z > L$ begins to lose its intensity, but the same occurs for the field within the range of $0 \leqslant z \leqslant L$, an undesired result. In Fig. 2(d) the resulting beam is strongly affected by the narrow width of the Gaussian apodization and the desired intensity pattern in the range of $0 \leqslant z \leqslant L$ is not obtained even in an approximate form.

In summary, we see that the proposed solution [Eq. (20)] can reproduce the desired longitudinal intensity pattern within $0 \leqslant z \leqslant L$ only when large values of the Gaussian apodization width are chosen.[3] But, unfortunately, this results in increased undesired residual intensities in the $z > L$ range, which is a consequence of the periodicity of the original FW in lossless media. Of course, to decrease these undesired residual intensities after $z = L$, one may use smaller values for the Gaussian apodization width. But, unfortunately, this in turn spoils the field to be reproduced within $0 \leqslant z \leqslant L$ due to the natural decay of the BG beam intensity along the propagation direction. This intensity decay occurs even in the absence of material absorption, as is the case for the current example. For (20) to be able to represent the beams with the desired properties, some changes must be implemented. The next section is devoted to these changes.

[3]That is, values for the Gaussian apodization widths much greater than the spot size of the FW which is being apodized, i.e., $\Delta\rho_G = 1/\sqrt{2}q \gg r_0$.

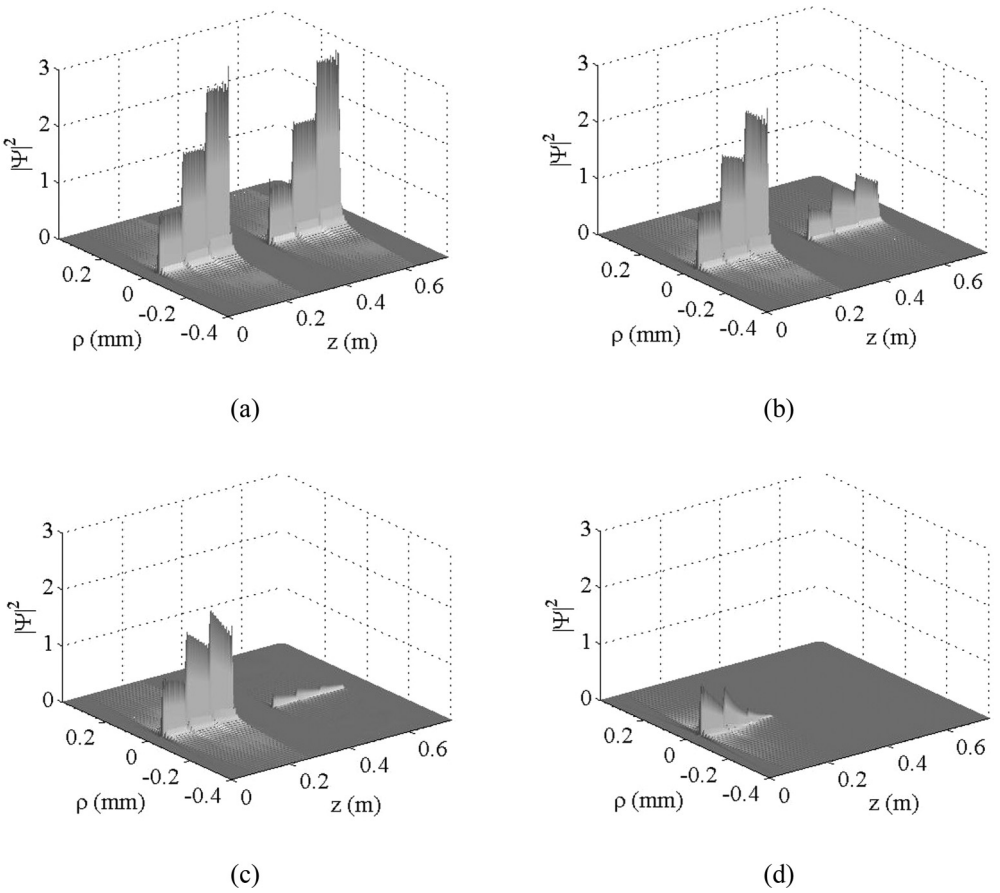

FIG. 2. Figures show apodized Bessel-Gaussian FW in a lossless medium with increasing values for the apodization width ($\Delta\rho_G$). (a) $\Delta\rho_G = 10^4\, r_0$, (b) $\Delta\rho_G = 800\, r_0$, (c) $\Delta\rho_G = 500\, r_0$, and (d) $\Delta\rho_G = 200\, r_0$. For large values of $\Delta\rho_G$, FWs display an undesired periodicity along the direction of propagation, whereas for small values of $\Delta\rho_G$ the beam pattern within the target region $0 \leqslant z \leqslant L$ loses its intensity.

IV. MODELING THE INTENSITY PATTERN OF FINITE-ENERGY DIFFRACTION- AND ATTENUATION-RESISTANT BEAMS IN ABSORBING MEDIA: FWS FROM BESSEL-GAUSS BEAM SUPERPOSITION

In this section we show that a finite-power, analytical, FW solution without spatial periodicity along the direction of propagation is possible by using Eq. (20), provided some modifications to the coefficients A_n and a suitable redefinition of the intensity pattern function, $|F(z)|^2$, and its domain are made. To discuss these modifications, a better understanding of the terms appearing in Eq. (20) is needed.

A Bessel-Gauss beam is the result of an apodization made with a Gaussian $\exp(-q^2\rho^2)$ on a Bessel beam $J_\nu(\eta\rho)\exp(i\nu\phi)\exp(i\zeta z)\exp(-i\omega t)$, at the initial $z = 0$ plane. It can be calculated, in the paraxial approximation, from the Fresnel diffraction integral [10–14], resulting in

$$\psi_{BGb}(\rho,z,\phi,t) = e^{ikz}\, e^{-i\omega t}\, \frac{\exp\left(-q^2\frac{\rho^2}{\mu}\right)}{\mu}\, J_\nu\left(\eta\frac{\rho}{\mu}\right) e^{i\nu\phi} \times \exp\left(-i\frac{\eta^2}{2k}\frac{z}{\mu}\right), \tag{21}$$

where μ is given by Eq. (14) and, as before, the complex wave number (k) is given by Eq. (3). Moreover, the spot radius of an ideal Bessel beam is given by $\Delta\rho_{Bb} \approx 2.4/\eta$ and the transverse intensity width of the Gaussian apodization at $z = 0$ is $\Delta\rho_G = 1/\sqrt{2}q$.

Now, a necessary condition for the Bessel-Gaussian beam to display a diffraction resistance behavior,[4] in the sense of preserving its spot size over long distances, is $\Delta\rho_G \gg \Delta\rho_{Bb} \Rightarrow \eta \gg q$. Moreover, based on the results of [11,12] a conservative estimate of the diffraction resistance distance (Z_{BG}) of a Bessel-Gauss beam is

$$Z_{BG} \approx \frac{k_r}{q\eta}. \tag{22}$$

In terms of the beam's attenuation, the product $\exp(ikz)\exp(-i\eta^2 z/2k\mu)$ in Eq. (21) is the main factor responsible for the beam's intensity degradation. More specifically, the intensity decrease is dictated by the function $G^2_{BG} \equiv |\exp(ikz)\exp(-i\eta^2 z/2k\mu)|^2$, where by using (14) we have

$$G_{BG}(z) = e^{-k_i z}\exp\left(\frac{-\eta^2(k_i + 2q^2 z)z}{2[k_r^2 + (k_i + 2q^2 z)^2]}\right). \tag{23}$$

[4]Note that we are saying that the Bessel-Gauss beam's diffraction resistance is related to its ability to maintain its spot size, not its intensity, which starts decreasing from the beginning even in a lossless medium.

Moreover, we note that Eq. (20) is a superposition of Bessel-Gauss beams with different transverse wave numbers given by (15). Each of the Bessel-Gauss terms in the superposition possesses a different diffraction resistance distance and intensity decreasing factor, according to (22) and (23). However, the differences among these transverse wave numbers are, in general, very small. This comes about because, in the context of the paraxial approximation, the beam spot size has to be much greater than the wavelength of operation, i.e., $r_0 \gg \lambda$. This condition implies that the value of the parameter Q will be smaller, but still close to $k_r = n_r\omega/c$. This fact, along with Eqs. (16), (18), and (19), allows us to affirm that

$$\frac{\eta_{-N} - \eta_N}{\eta_0} \ll 1, \tag{24}$$

i.e., there are just small differences among the $2N+1$ transversal wave numbers η_n of the Bessel-Gauss beams in superposition (20). With this result at hand, we can say that the diffraction resistance distances and the intensity decreasing factor of all Bessel-Gauss beams in superposition (20) are determined, approximately, by

$$Z \approx \frac{k_r}{q\eta_0} \tag{25}$$

and

$$G(z) \approx e^{-k_i z} \exp\left(\frac{-\eta_0^2(k_i + 2q^2 z)z}{2\left[k_r^2 + (k_i + 2q^2 z)^2\right]}\right). \tag{26}$$

Equations (25) and (26) are important results as will be seen in the following discussions.

Finally, we achieve the goal of obtaining finite power, analytical, FW solutions without spatial periodicity along the direction of propagation by implementing the five steps listed below. The required changes for coefficients A_n and the suitable redefinition of $F(z)$ and its domain are introduced and discussed in the second and fifth steps.

Step 1. We assume a FW solution of the form Eq. (20).

Step 2. Once the desired intensity pattern $|F(z)|^2$ is chosen for a given longitudinal spatial range, we proceed to write such a range as $0 \leqslant z \leqslant L/2$. In addition, we extend the domain of $F(z)$ to $0 \leqslant z \leqslant L$, demanding null values for this function in the extended range $L/2 < z \leqslant L$.

Mathematically, we demand that $\Psi(\rho = \rho_0, \phi, z, t) \approx |F(z)|^2$ within $0 \leqslant z \leqslant L$, being

$$F(z) = \begin{cases} F(z) & \text{for } 0 \leqslant z \leqslant L/2, \\ 0 & \text{in } L/2 < z \leqslant L. \end{cases} \tag{27}$$

The added region $L/2 < z \leqslant L$ ensures that $F(z)$ has small values in that range, while to further ensure very low intensity for $z > L$, it is necessary to choose a suitable value for the parameter q, as discussed in step 4.

Step 3. The values of the transverse and longitudinal wave numbers, η_n and ζ_n, are given by Eqs. (16) and (18), respectively. The value of Q can be obtained from Eq. (8) or (9), depending on whether we wish to model the beam patterns on the z axis or on the surface of the axial cylinder, respectively. The maximum value of N, which defines the maximum number of terms $(2N+1)$ in the superposition (20), can be obtained from (19). Of course, one is not obligated to use the maximum value of the N, but just enough to obtain a good result.

Step 4. The value of the parameter q is chosen according to

$$q = \frac{2k_r}{L\,\eta_0}. \tag{28}$$

This choice for q ensures that all Bessel-Gauss beams in the superposition (20) arrive at $z = L/2$ keeping their nondiffracting characteristics, even if suffering a decrease in their intensities by a factor of approximately $\exp(k_i L)\exp(2)$. At the same time, this choice ensures that at $z = L$ the intensities of the beams have decreased approximately by a factor of $\exp(2k_i L)\exp(8)$, so that the resulting superposition is vanishingly small for $z > L$.

Step 5. The new form of the coefficient A_n to be used in superposition (20) is now given by

$$A_n = \frac{1}{L}\int_0^L \frac{F(z)}{G(z)}\, e^{-i\frac{2\pi}{L}nz} dz. \tag{29}$$

The reason for this change is the fact that by using the old form [Eq. (6)] in (20) the resultant FW does not have the desired pattern $[|F(z)|^2]$ in the range $[0, L/2]$. In fact, the pattern is attenuated by the square of the second exponential term in (26). In effect what we have done is a compensation scheme: the new coefficients A_n in (29) result in a beam whose (on axis) intensity is approximately $|F(z)/G(z)|^2 \times |G(z)|^2 = |F(z)|^2$, which is the desired longitudinal intensity pattern.

Steps 1 through 5 discussed above can now be used to obtain a finite-energy version of the FW solution. However, before demonstrating this via an example, we would like to comment on a useful simplification that can be used to evaluate (29). Because of not so simple form of the $G(z)$ in (26), integral in Eq. (29) can be difficult to evaluate analytically. Of course, one can always rely on numerical integration to calculate (29); but since we have been working toward obtaining an analytical FW solution with finite power, let us keep this character of the solution by obtaining an approximate expression for (29).

For a medium with moderate absorption, i.e., $k_r \gg k_i$, and assuming $\eta_0 \gg q \gg k_i$, and taking into account that in (29) the contributions to the integral occur only within the range of $0 \leqslant z \leqslant L/2$, it can be shown that

$$G(z) \approx e^{-k_i z} \exp\left(\frac{-\eta_0^2 q^2 z^2}{k_r^2}\right). \tag{30}$$

This implies that

$$G^{-1}(z) \approx e^{k_i z} \exp\left(\frac{\eta_0^2 q^2 z^2}{k_r^2}\right) = e^{k_i z} \sum_{m=0}^{\infty} \frac{\chi^m}{m!}, \tag{31}$$

where

$$\chi = \frac{\eta_0^2 q^2 z^2}{k_r^2}. \tag{32}$$

Integral in (29) can now be written as

$$A_n \approx \frac{1}{L}\int_0^L \left(\sum_{m=0}^{\infty} \frac{\chi^m}{m!}\right) e^{k_i z} F(z)\, e^{-i\frac{2\pi}{L}nz} dz. \tag{33}$$

In conclusion, for a given intensity pattern $|F(z)|^2$, if Eq. (6) can be analytically evaluated, Eq. (33) can also be calculated analytically.

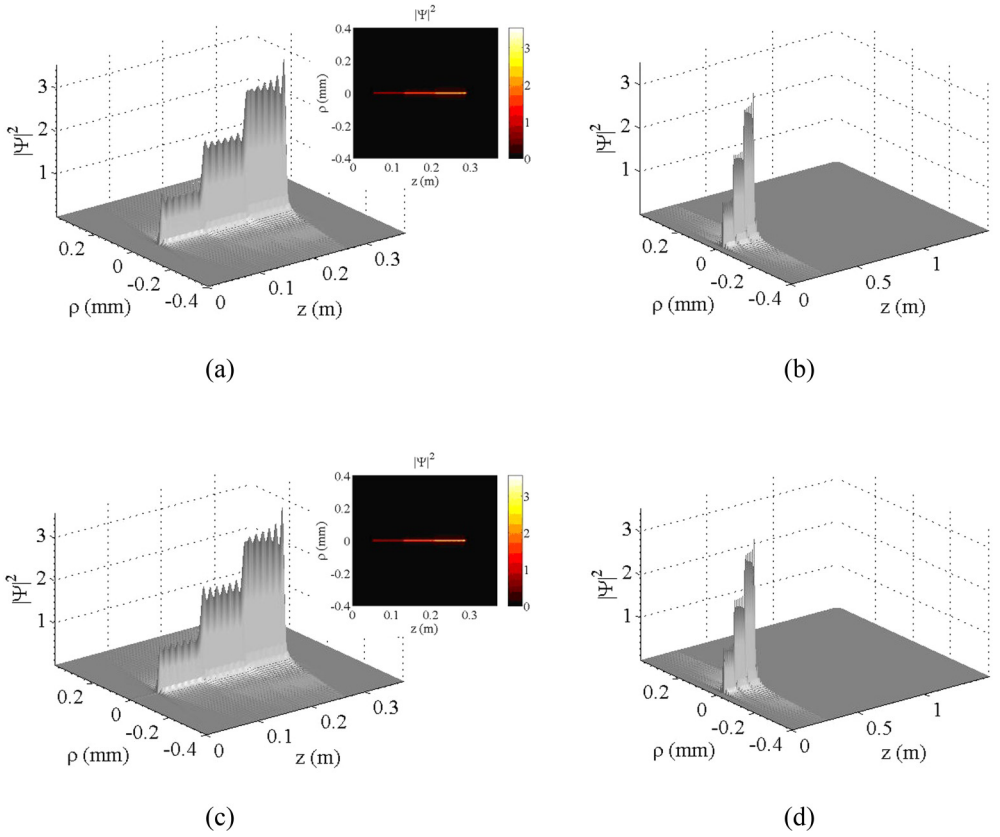

FIG. 3. (Color online) (a) Finite-energy FW with a step function longitudinal (on-axis) intensity pattern in the nonabsorbing medium and its orthogonal projection in the detail. (b) The same beam within the longitudinal range $0 \leqslant z \leqslant 2L = 1.48$ m, where we can see there is no spatial (longitudinal) periodicity. (c) A finite-energy FW representing the desired diffraction- and attenuation-resistant beam in the absorbing medium and the orthogonal projection in the detail. (d) The same beam within the longitudinal range $0 \leqslant z \leqslant 2L = 1.48$ m.

In many situations it can occur that $\chi < 1$ within the range $0 \leqslant z \leqslant L/2$ and, in these cases, it is enough to consider just a few terms of the power series in (33). In the following, to illustrate the efficiency of this method, we apply it to the example 1 of the first section.

A. Example

Example 3. We wish to use our solution (20) to obtain two finite-energy diffraction- and attenuation-resistant beams, one of them in a nonabsorbing medium with $n_{\text{ref}} = n_r = 2$ and the other one in an absorbing medium with $n_{\text{ref}} = n_r + in_i = 2 + i\,7.5 \times 10^{-7}$, both beams at $\lambda = c/f = 632.8$ nm, possessing the same spot size of radius $r_0 \approx 9\ \mu$m and with the same ladder-shaped longitudinal (on-axis) intensity pattern within the range $0 \leqslant z \leqslant L/2 = 0.37$ m, similar to that of the first example of Sec. I, with negligible intensity in $z > L/2$. Therefore, according to step 2, we demand that $|\Psi(\rho = 0,\phi,z,t)|^2 \approx |F(z)|^2$ within $0 \leqslant z \leqslant L$, being $F(z)$ given in this range by

$$F(z) = \begin{cases} 0 & \text{for } 0 \leqslant z < l_1, \\ 1 & \text{for } l_1 < z < l_2, \\ \sqrt{2} & \text{for } l_2 < z < l_3, \\ \sqrt{3} & \text{for } l_3 < z < l_4, \\ 0 & \text{for } l_4 < z \leqslant L/2, \\ 0 & \text{for } L/2 < z \leqslant L, \end{cases} \tag{34}$$

where $l_1 = 0.05$ m, $l_2 = l_1 + \delta z$, $l_3 = l_2 + \delta z$, and $l_4 = l_3 + \delta z$, with $L = 2 \times 0.37$ m $= 0.74$ m and $\delta z = 0.08$ m.

Now, for both beams, we proceed to implement Steps 3, 4, and 5, obtaining ζ_n, η_n, Q, q, and A_n. We note that in this example it is possible to obtain very good approximations for the values of A_n through Eq. (33) by considering just four terms in the series appearing in that integrand. We also note that for both beams the maximum value to N is 210, and we have chosen to use $N = 60$.

The resulting finite power FWs beam's intensities are shown in Fig. 3. Figures 3(a) and 3(b) show the case of nonabsorbing medium considering different longitudinal distances, $0 \leqslant z \leqslant L/2 = 0.37$ m and $0 \leqslant z \leqslant 2L = 1.48$ m, respectively. We can see the diffraction-resistant beam with the desired longitudinal intensity pattern occurring within the chosen longitudinal range and, as desired, very low intensities after it.

Figures 3(c) and 3(d) show the absorbing medium case, considering different longitudinal distances, $0 \leqslant z \leqslant L/2 = 0.37$ m and $0 \leqslant z \leqslant 2L = 1.48$ m, respectively. We can see that the desired diffraction- and attenuation-resistant beam (carrying finite power) is obtained within the chosen longitudinal range, with very low intensities after it.

For a better visualization of the nondiffracting character of both beams above, Fig. 4 shows a zoom-in on the orthogonal

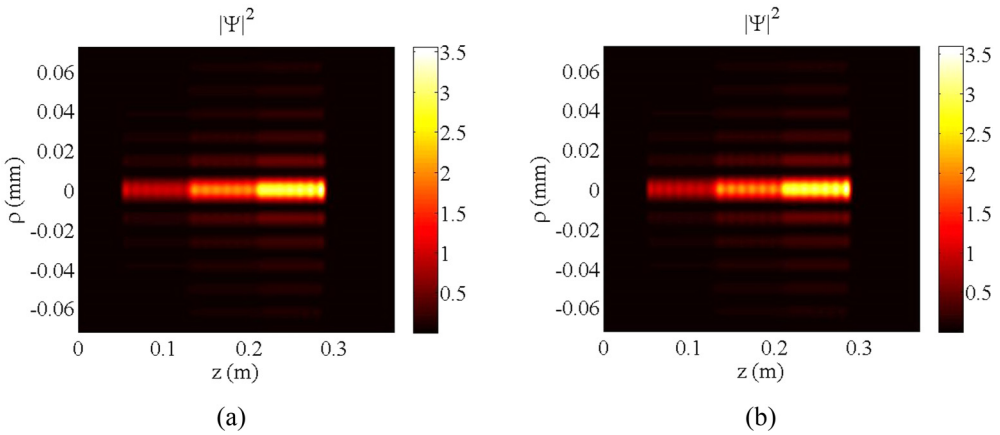

FIG. 4. (Color online) Zoom-in on the orthogonal projections of the beam's intensities in the cases of (a) nonabsorbing medium and (b) absorbing medium.

projections of their intensities on the plane (ρ, z). Figure 4(a) corresponds to the nonabsorbing case and Fig. 4(b) to the absorbing one.

The beams in the two media are very similar, showing the high efficiency of the method.

At this point we wish to make some remarks about the limits of the depth of field of these beams and their experimental implementation.

With regard to the resistance to the diffraction effects (i.e., the maintenance of the spot radius r_0), the method can provide diffraction resistance distances arbitrarily greater than that of the ordinary beams ($k_r r_0^2$) just by increasing the initial width of the Gaussian apodization through an appropriate choice of the parameter q via Eq. (28). Naturally this implies increasing the energy and the size of the aperture required to generate the desired beam.

The situation with relation to the attenuation (absorption) is not so simple. It should be clear that the energy absorption by the medium continues to occur normally, the difference is that the present beams have a sophisticated initial transverse field pattern capable of reconstructing their central cores till a certain distance. This process demands energy and there is, of course, a limitation on the depth of field of these beams. According to the several cases we have studied, our method can provide beams resistant to attenuation for distances 10 to 15 times the penetration depth $(1/2k_i)$ of an ordinary beam. For distances longer than this, besides a greater energy demand, eventually it occurs that the field intensity in the lateral regions becomes even higher than that of the core, a nondesirable effect.

Now, concerning the experimental generation of the diffraction- and attenuation-resistant beams, one could use, for instance, computer generated holograms (CGH) optically reconstructed by Spatial Light Modulators (SLMs). This technique was already used with success in [5,6] for the generation of FWs in a nonabsorbing medium (air). More specifically, with the analytical solution of the desired beam in hand, the information about its amplitudes and phases at the initial plane can be used to construct the complex transmittance hologram function and perform the amplitude CGH. In this case, the efficient generation of the beam depends on the SLM resolution: the phase and amplitude of the signal used to create the CGH should not change significantly within spatial intervals of the order of the SLM resolution.

V. CONCLUSIONS

In this paper we develop a method, based on suitable Bessel-Gauss beam superposition, capable of providing finite-energy versions of the Frozen Waves beams in material absorbing media. From this approach, we can obtain diffraction- and attenuation-resistant beams whose longitudinal intensity pattern can be chosen *a priori*. This intensity pattern can be concentrated over the z axis, with a beam of spot size r_0, or over a cylindrical surface of radius ρ_0.

The method also guarantees a negligible field intensity after the region where the desired field is localized, thus ensuring finite-power flux to the resulting beam and eliminating, in the case of lossless media, the undesirable problem of the periodic field intensity of the original FWs.

The results here exposed are of theoretical interest, as they allow the analytical description of finite energy and spatially shaped diffraction- and attenuation-resistant beams, showing how a base constituted of Bessel-Gauss beams can be useful, and also of practical interest, as they facilitate the predictions of the experiments aimed for generating such beams, which can be useful in many applications, as in optical tweezers, optical atom guiding, remote sensing, free space optics communications, etc.

It is worth noting that we are currently involved in the experimental verification of the present paper.

ACKNOWLEDGMENTS

The authors would like to thank Erasmo Recami and Ioannis M. Besieris for valuable discussions and kind collaboration. Thanks are also due to partial support from FAPESP (under Grant No. 2013/26437-6) and from CNPq (under Grant No. 312376/2013-8).

[1] M. Zamboni-Rached, Diffraction-Attenuation resistant beams in absorbing media, Opt. Express **14**, 1804 (2006).

[2] M. Zamboni-Rached, L. A. Ambrósio, and H. E. Hernández-Figueroa, Diffraction–attenuation resistant beams: their higher-order versions and finite-aperture generations, Appl. Opt. **49**, 5861 (2010).

[3] *Localized Waves*, edited by H. E. Hernández-Figueroa, M. Zamboni-Rached, and E. Recami, Wiley Series in Microwave Optical Engineering (Wiley, Hoboken, NJ, 2007).

[4] *Non-Diffracting Waves*, edited by H. E. Hernández-Figueroa, Erasmo Recami, and M. Zamboni-Rached (Wiley-VCH, Weinheim, Germany, 2014).

[5] T. A. Vieira, M. R. R. Gesualdi, and M. Zamboni-Rached, Frozen waves: experimental generation, Opt. Lett. **37**, 2034 (2012).

[6] T. A. Vieira, M. Zamboni-Rached, and M. R. R. Gesualdi, Modeling the spatial shape of nondiffracting beams: Experimental generation of Frozen Waves via holographic method, Opt. Commun. **315**, 374 (2014).

[7] C. A. Dartora, K. Z. Nóbrega, A. Dartora, G. A. Vianad, H. Tertuliano, and S. Filho, Study of Frozen Waves theory through a continuous superposition of Bessel beams, Opt. Laser Technol. **39**, 1370 (2007).

[8] J. C. Gutiérrez-Vega and M. A. Bandres, Helmholtz-Gauss waves, J. Opt. Soc. Am. A **22**, 289 (2005).

[9] M. Guizar-Sicairos and J. C. Gutiérrez-Vega, Propagation of Helmholtz-Gauss beams in absorbing and gain media, J. Opt. Soc. Am. A **23**, 1994 (2006).

[10] A. P. Kiselev, New structures in paraxial Gaussian beams, Opt. Spectrosc. (USSR) **96**, 479 (2004).

[11] F. Gori and G. Guattari, Bessel-Gauss beams, Opt. Commun. **64**, 491 (1987).

[12] D. N. Schimpf, J. Schulte, W. P. Putnam, and F. X. Kärtner, Generalizing higher-order Bessel-Gauss beams: analytical description and demonstration, Opt. Express **20**, 26852 (2012).

[13] G. Wu, F. Wang, and Y. Cai, Generation and self-healing of a radially polarized Bessel-Gauss beam, Phys. Rev. A **89**, 043807 (2014).

[14] D. Madhi, M. Ornigotti, and A. Aiello, Cylindrically polarized Bessel-Gauss beams, J. Opt. **17**, 025603 (2015).